Enhancing Material Thickness Measurement: Ultrasonic Sensor Data Analysis and Thickness Prediction Using Neural Networks

Vahid Hassani*, Antonis Porichis, Farhan Mahmood and Panagiotis Chatzakos

University of Essex, AI Innovation Centre, National Structural Integrity Research Centre (NSIRC), Great Abington, Cambridge CB21 6AL, UK

*Corresponding author: v.hassani@essex.ai

Copyright © 2024 The Authors.

Abstract: Accurate and non-invasive measurement of material thickness plays an important role across several industry sectors such as aerospace, oil and gas, rail and others. This paper aims to use neural networks as a predictive tool to enhance thickness measurement accuracy of immersed steel samples. In this study, a set of training data is provided through conducting experiments on an immersed wedge sample with varying thickness using the A-scan method. This dataset is used for training a single-layer neural network. To evaluate the performance of the trained neural network, a set of test data is provided on different samples with various thicknesses. Through this study, a promising methodology is demonstrated toward accurate and effective thicknesses prediction using neural networks. The outcomes exhibited good agreement when employing a neural network with the same architecture to predict the void locations in another sample of similar material. Furthermore, the results revealed that this method has achieved an error of less than 3% for thickness prediction and less than 7% for void detection.

Keywords: Data cleaning process; Neural networks; Thickness prediction; Ultrasonic sensor.

1. INTRODUCTION

The accurate measurement of material thickness is an important assignment in several industry sectors, ranging from manufacturing to oil and gas. Conventional methods of thickness prediction and estimation are error-prone, time-consuming, and sometimes intrusive. The emergence of ultrasonic sensors as promising tools for non-destructive testing (NDT) has enabled engineers and researchers to attain more accurate and real-time monitoring capabilities [1]. On the other hand, the progress in machine learning techniques, especially artificial neural networks have enabled for the development of efficient predictive tools to estimate the vital parameters of an object in the areas where the direct measurement is not possible.

Ultrasonic thickness measurement utilises the principle of sound wave propagation through materials. This measurement is done by ultrasonic sensors in which the key element is a piezoelectric transducer [2, 3]. Calculating the thickness of a sample using immersion ultrasonic testing involves measuring the time it takes for an ultrasonic pulse to travel through the sample and be reflected to the sensor [4]. When an ultrasonic pulse is emitted from a transducer, it travels through the material and reflects from the opposite surface. By analysing the time taken for the echo to return, the thickness of the material can be accurately calculated using the speed of sound in the material. In the immersed condition, by knowing the speed of sound in the liquid and the time taken for the round-trip travel of the ultrasonic pulse, one can determine the liquid gap between the sensor and the upper surface of the sample. This technique eliminates the need for physical contact and provides measurements that are not affected by surface conditions, making it highly suitable for a wide range of applications such as detecting the corroded surfaces under the water and internal voids in the object. In this context, some methods have been proposed by researchers to estimate the thickness of the immersed objects for NDT purposes. An NDT method using ultrasonic technology was presented to measure layer thickness in water-assisted coinjection molding (WACIM) parts, basically to determine layer thickness variations effectively and offering potential applications in polymeric part quality assessment [5]. Ultrasonic NDT is also utilised to estimate the thickness of coatings on ships and marine structures due to its convenience and speed, but challenges in underwater environments were overcome by designing a water delay line using reflection coefficients and evaluating time-of-flight (ToF) on the reflected echo, which result in more accurate measurements with lower errors compared to calliper measurements [6]. Alternatively, a method was presented for real-time estimation of thick oil slick volume, which is essential for oil spill response planning [7]. In a different application, to prevent accidents in nuclear power plants due to pipe damage from corrosion and erosion, it is quint essential to investigate pipe wall thickness non-destructively and predict remaining pipe life. However, the study enumerates that the inherent uncertainty in NDT results that has to be considered in

developing a reliable pipe wall thinning management system. The proposed method accounted for this uncertainty and proved highly accurate in predicting wall thickness compared to conventional methods [8].

In terms of using various methods to estimate the thickness by ultrasonic measurement, a new approach was introduced using the Unscented Kalman Filter (UKF) combined with a Sliding Mode Observer (SMO), to effectively process electromagnetic ultrasonic signals for measuring pipeline wall thickness [9]. Experimental results on a number of samples demonstrated that the proposed method improves the signal-to-noise ratio up to 171% compared to other methods, and a proposed random-based technique reduces overall filtering time. As a functional tool, an inductively coupled ultrasonic transducer system (ICTS) can be used for measuring wall thickness in the structural health monitoring framework. To optimise the results of measurement, a correction algorithm was developed to enhance its precision, reduce measurement variability from 0.19 mm to 0.07 mm and enabled for accurate thickness measurement even within up to 20 mm lateral and 10 mm vertical misalignment, to make it suitable for manual and future robotic inspections [10]. Besides A-scan, B-scan and C-scan methods are also widely used in different industry sectors because of offering higher resolutions and accuracy [11]. For instance, the development of an ultrasonic immersion C-scan testing system for industrial and metrological applications uses software that allows for automatic sample scanning with user-specified parameters, achieving a defect location detection resolution of ±0.01 mm and high-quality image generation due to a transducer movement resolution of ±0.01 mm [12].

The neural networks as a useful tool for predicting the time series data allows for implementing a data-driven approach to predict and analyse material thickness using ultrasonic measurement [13]. Neural networks deliver a set of algorithms applied for image and data processing which has been inspired by the structure of the human brain, capable of learning complex patterns through exploring relationships from data [14]. When neural networks are integrated into time-series data collected from ultrasonic sensors, it can learn the intricate correlations between signal patterns and corresponding material thicknesses. This predictive capability facilitates real-time monitoring purposes [15, 16]. Due to this unique capability, neural networks have a lot of industrial and engineering applications. As an example of an engineering application of neural networks, the importance of predicting the performance and lifespan of direct-drive electro-hydraulic servo valves was investigated in aerospace control systems to prevent accidents and economic losses due to performance degradation [17]. In this context, a method for aero-engine remaining life prediction was introduced, that included timing, invalid data, and deep feature extraction challenges. By employing time-series residual neural networks with temporal and deep feature extraction layers, accurate predictions were obtained using NASA's C-MAPSS dataset and superior performance was observed in comparison with other networks [18]. In recent years, long-short term memory (LSTM) networks have demonstrated good performance in the prediction of time-series data. The effectiveness of using a LSTM neural network to predict complex dynamical systems from time series data was proven in reproducing periodic orbits and short-term chaotic trajectories within capturing the long-term ergodic behaviour despite the sensitivity to initial conditions and increasing uncertainty in chaotic data series [19]. Repeatedly, a LSTM network was developed to predict leakage pressure in the complex geological structures of the Shunbei Oilfield [20]. In an innovative manner, composite neural networks can improve the prediction performance of time-series data significantly. These networks are usually developed by coupling LSTM networks with convolutional neural networks (CNN) and recurrent neural networks (RNN) [21, 22].

Understanding the unique capabilities of neural networks, specifically designed for complex ultrasound pattern recognition [23], this study proposes a novel data-driven approach to accurately predict material thickness and detect voids using ultrasonic sensor data. Traditional methods often rely on analysing the entire time-series data, which can be computationally intensive and prone to noise interference. However, the innovation in this research lies in utilising the time difference between consecutive peaks in the ultrasonic signal output. This approach effectively reduces the amount of input data required for analysis while preserving critical information for accurate prediction. By focusing on specific features of the signal rather than the whole data, the proposed methodology streamlines the process and enhances the efficiency of thickness measurement and void detection for real-time measurement.

2. EXPERIMENT

This section describes the experimental configuration designed for ultrasonic testing of several steel samples conducted both underwater and in a non-submerged environment. The objectives of this section include:

    a.   To assess the appropriate range of sensor bandwidth for thickness measurement via contact testing conducted outside the water.
    b.   To validate the accuracy of the sensor and experimental setup for underwater testing.
    c.   To evaluate the data quality obtained from the sensor and oscilloscope.
    d.   To generate a dataset to train the neural nwteorks model in the subsequent sections.

The experiment is carried out utilising an experimental set-up as shown in Figure 1, incorporating a cylindrical sensor, sensor holder and sensor gland. This sensor is utilised for both contact testing outside the water container and non-contact testing within the container. Notably, the cylindrical sensor utilised in this experiment is the H5M model, possessing a bandwidth of 5 MHz and a diameter of 10 mm.

Figure 2 illustrates the entire experimental configuration devised for facilitating both contact and non-contact ultrasonic experiments. Considering this setup, a pulse generator produces pulses at varying frequencies for the sensor, while a power source provides the necessary power for the pulse generator's operation. The role of the pulse generator is to amplify the input voltage to capture the robust signal from the reflected wave emanating from the samples. An oscilloscope is employed to observe and save the data received from the sensor via pulse generator for subsequent analysis. Typically, the oscilloscope presents the waveform of the received ultrasonic voltage signal, represented as a sequence of peaks and valleys.
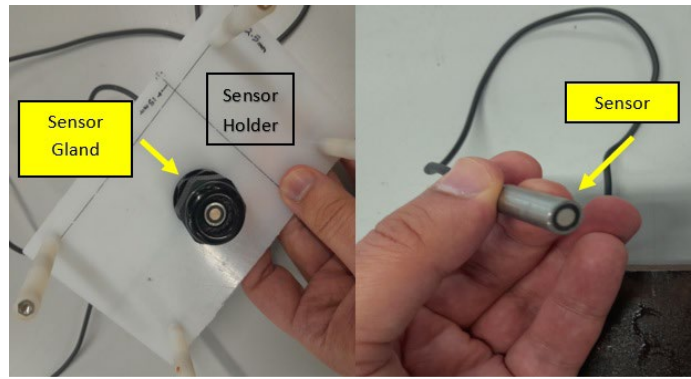
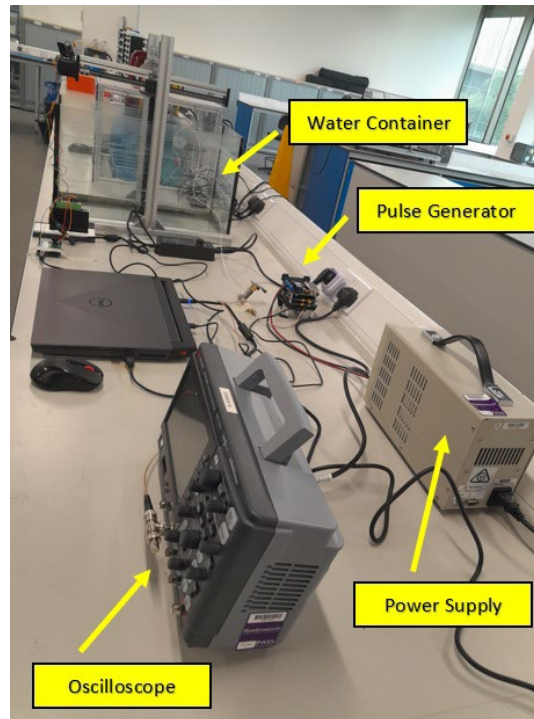Figure 1. Cylindrical sensor with 5 mm diameter (H5M with 5 MHz bandwidth).

Figure 2. Experimental setup.

To identify the peaks and valleys in the waveform, we need to identify the following key points (shown in Figure 3) on the oscilloscope screen or any other monitoring devices:
   a.   First valley (initial pulse in Figure 3): It corresponds to the initial emission of the ultrasonic pulse.
   b.   Second valley (t_1 in Figure 3): It represents the point where the ultrasonic pulse is first reflected from the top surface of the sample.
   c.   Third valley (t_2 in Figure 3): It corresponds to the reflection when the ultrasonic pulse returns to the sensor after traveling from the back-wall of the sample.

2.1 Contact Test Outside the Water Container

To conduct this experiment, it is essential to establish connections among the ultrasonic sensor, the oscilloscope, and the pulse generator. The pulse generator transmits signals to the sensor and receives the reflected signal from the sensor, which is then relayed to the oscilloscope for monitoring and recording purposes. It is necessary to meticulously align these devices before conducting the tests. In the case of the non-contact experiment, the sample must be laid in the water container, whereas for the contact test, it must make direct contact with the sensor using a liquid coupling. Additionally, the sensor has to be oriented perpendicular to the surface of the sample, as shown in Figure 4.

As mentioned in the beginning of this section, the objective of the contact test is to determine the sensor's ideal operational frequency bandwidth. As shown in Figure 5, this test helps identify the most suitable frequency bandwidth for the sensor, which is between 4.16 MHz and 7.15 MHz, with the example of 5 MHz being determined as the optimal frequency. This finding serves as a reference for configuring the pulse generator to transmit signals at the desired frequency to the sensor positioned beneath the water.
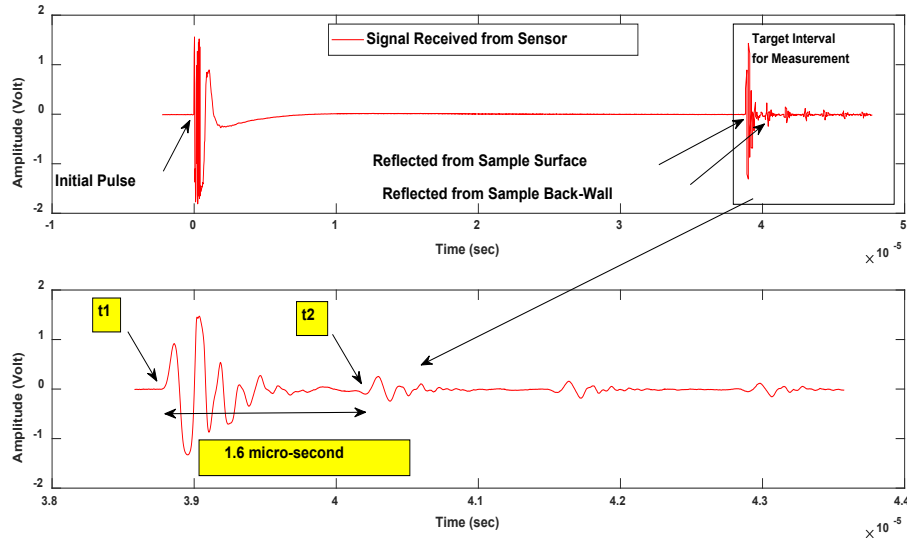
Figure 3. Signal received from the sensor underwater. t_1: The time at which the wave is reflected from sample surface; t_2: The time at which the wave is reflected from sample back-wall.
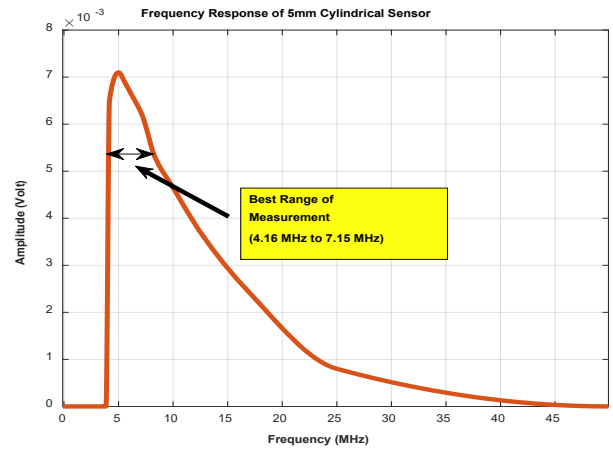

Figure 4. sensor in contact test.

Figure 5. Frequency response of the 5 mm sensor.

Using the time intervals (t_1 and t_2 as shown in Figure 3) measured between the key points on the oscilloscope, we can calculate the thickness (T) of the sample made of steel material in contact test outside the water container by using Equation (1),

$$T = (V_{steel} \times (t_2 - t_1))/2 \qquad (1)$$

where T is the thickness of the steel sample, V_{steel} is the speed of sound in steel, $(t_2 - t_1)$ is the time taken for the ultrasonic pulse to travel through the steel sample twice (seconds). This is the time difference between the second valley and the first valley. The speed of sound in steel varies depending on the steel's composition and properties. For general carbon steel and the samples used in this experiment, the speed of sound is around 5920 m/s. It should be noted that it is essential to ensure that the ultrasonic pulse travels through the steel sample at a near-perpendicular angle to obtain accurate results. Additionally, positioning and precise measurements are critical for reliable thickness determination.

2.2 Non-Contact Test Under the Water

In this test, the ultrasonic sensor emits an ultrasonic pulse that travels through the water medium, penetrates the steel sample, and then reflects to the sensor. Figure 6 illustrates the arrangements of sensor holders specifically designed for the 5 mm sensor, ensuring it remains submerged beneath the water and maintains a roughly consistent distance from the sample's top surface, which is known as water gap.

Calculating both the water gap distance and the steel sample's thickness becomes more intricate in this context. Here, we must account for the extra distance the ultrasonic pulse travels through the water-filled gap before entering and after exiting the steel sample. A detailed guide on how to calculate both the water gap and the thickness of the sample is as follows:
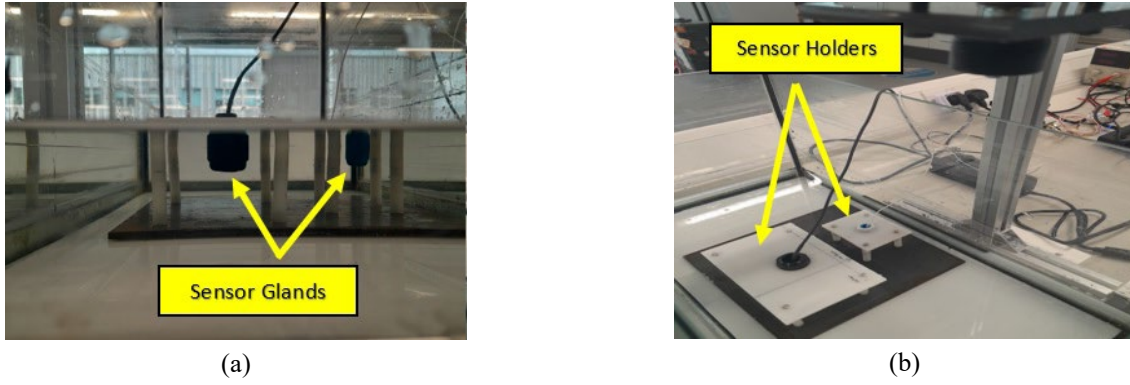
(a) (b)

Figure 6. Arrangement of the sensor holder, (a) Sensor glands; (b) Sensor holder (top-view).

a) Measure Time Intervals: Record the time intervals (referred to as t_1 and t_2) between the critical points present within the oscilloscope waveform, as explained previously. In Figure 3, both t_1 and t_2 are indicated for the responses captured from the sensor.

b) Calculate Water Gap Distance: Using the measured time interval (t_1), we are able to calculate the distance (D_W) travelled by the ultrasonic pulse through the water gap using the speed of sound in the water ($V_w = 1500$ m/s):

$$D_W = V_W \times \frac{t_1}{2} \qquad (2)$$

c) Calculate Effective Time of Flight: Determine the total time of flight of the ultrasonic pulse through both the water gap and the steel sample,

$$t_{total} = t_2 - t_1 \qquad (3)$$

d) Calculate Thickness: Finally, use the effective time of flight through the steel (t_s) to calculate the thickness (T) of the steel sample using the speed of sound in steel ($V_s = 5920$ m/s):

$$T = V_s \times {t_{total}}/{2} \qquad (4)$$

2.3 Wedge Test

This test is done to assess both the quality and precision of the signal received from the sensor underwater, as well as to evaluate the sensor's efficacy in detecting voids within the sample. For these purposes, a setup was dedicated using a wedge with varying thicknesses, ranging from 1 mm to 8 mm, as shown in Figure 7. The results, comparing the measured thickness with the expected values, are provided in Figure 8 and Table 1. As evidently appears, the differences between the measured values by the sensor and the known thicknesses of the wedge are exceptionally small in terms of percentage error. Figure 9 shows the plots obtained for the different amplitudes of the wedge sample.

A notch has been designed on the wedge to detect the void inside the sample by using the sensor. This notch has a 7.5 mm distance from the other side of the wedge as seen in Figure 10. This notch also was detected by installing the sensor on the other side of the wedge opposite to the notch side. The value of 7.6 mm was measured that proves the measurement error is 1.33%, which is negligible. Figure 11 shows the results of this measurement.
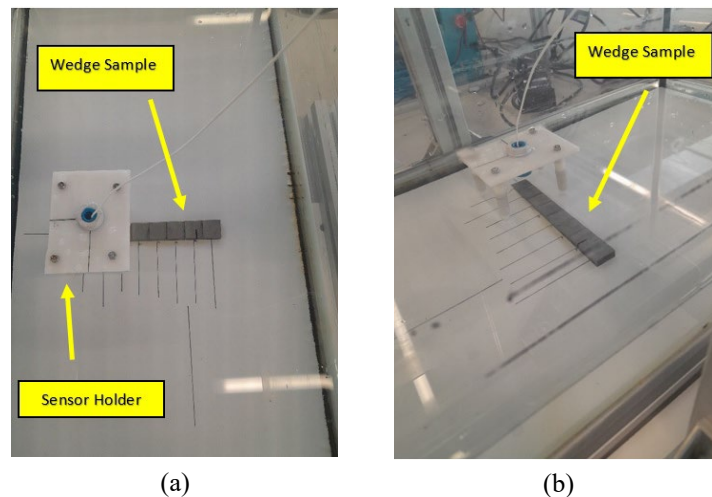

(a) (b)

Figure 7. (a) Wedge test (top view); (b) Wedge test (side view).

Table 1. Comparison between measured values by sensor and the nominal values of wedge thicknesses.

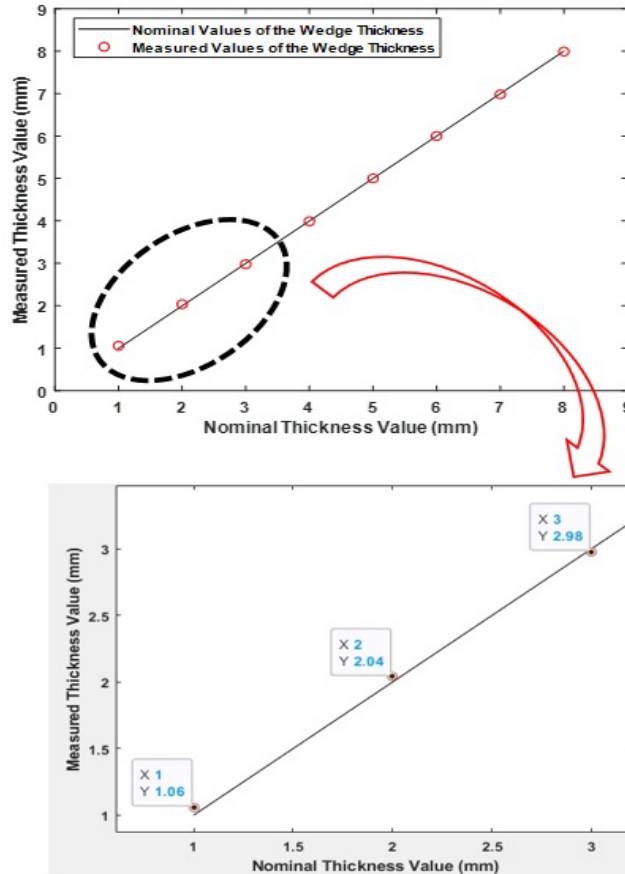| Nominal Values (mm)	Measured Values by Sensor (mm)	Error (%)
1	1.06	6
2	2.04	2
3	2.98	0.67
4	3.99	0.25
5	5.00	0
6	6.00	0
7	6.98	0.28
8	7.99	0.125

Figure 8. Comparison between measured values by sensor and the nominal values of wedge thicknesses.

(a)   (b)

(c)

(d)

(e)

(f)

(g)

(h)
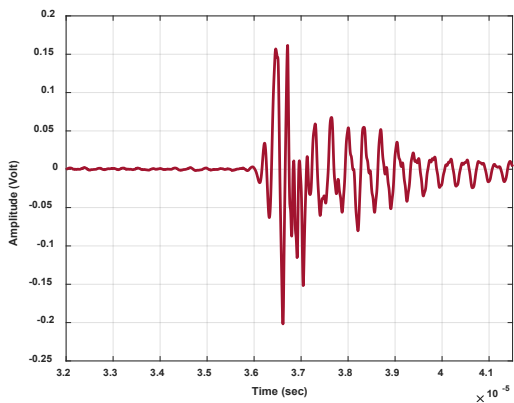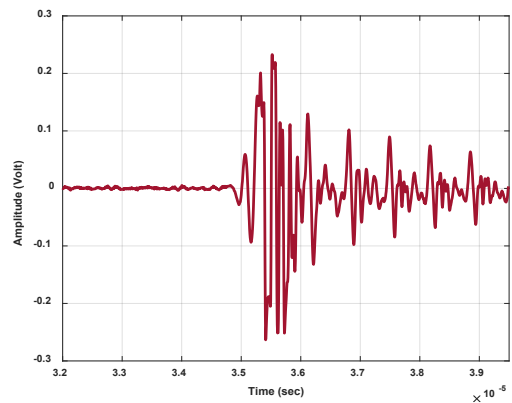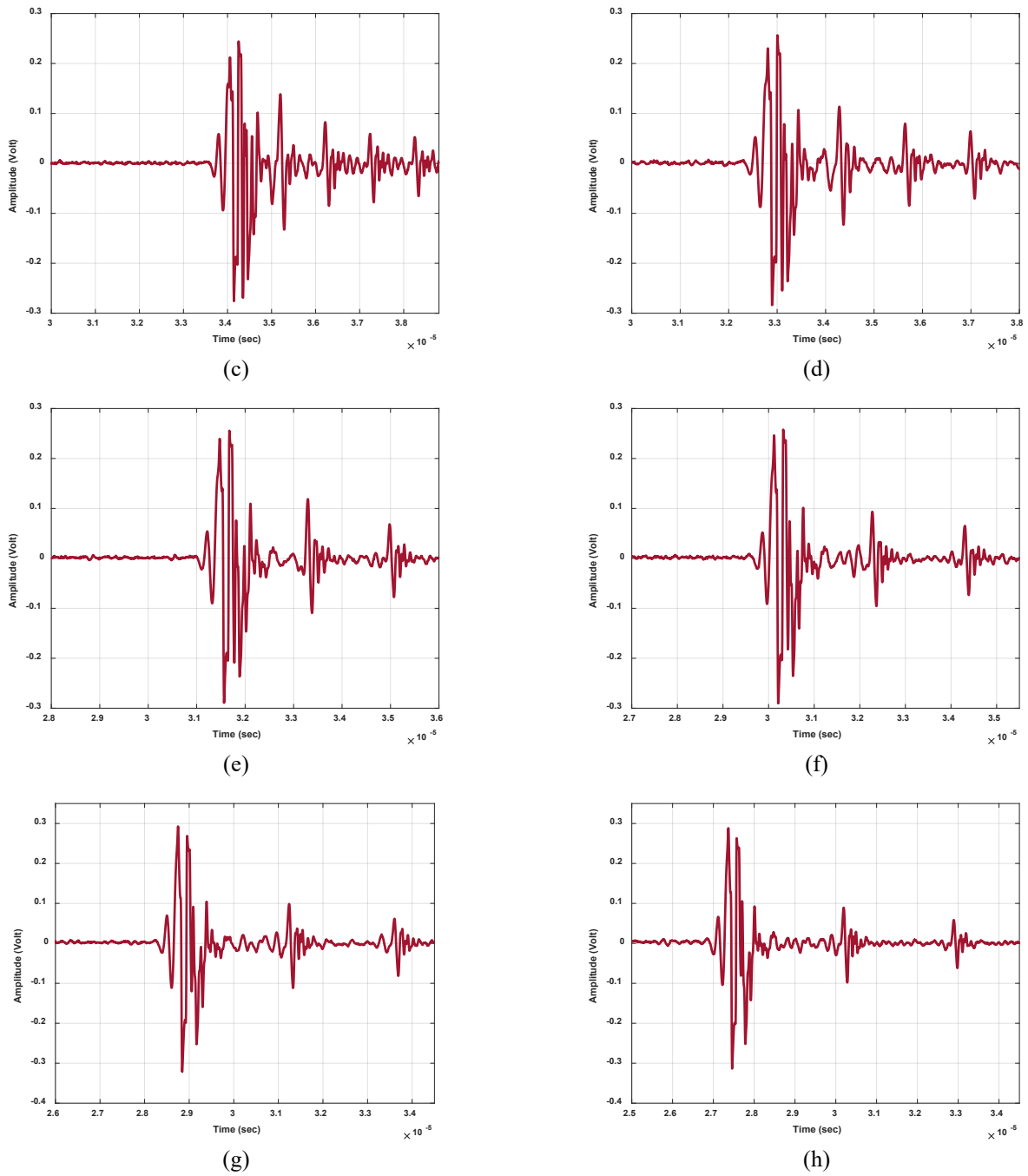
Figure 9. Results with different samples, (a) 1 mm; (b) 2 mm; (c) 3 mm; (d) 4 mm; (e) 5 mm; (f) 6 mm; (g) 7 mm; (h) 8 mm.
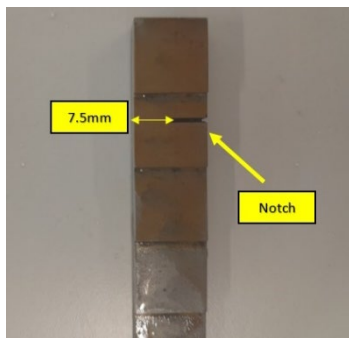

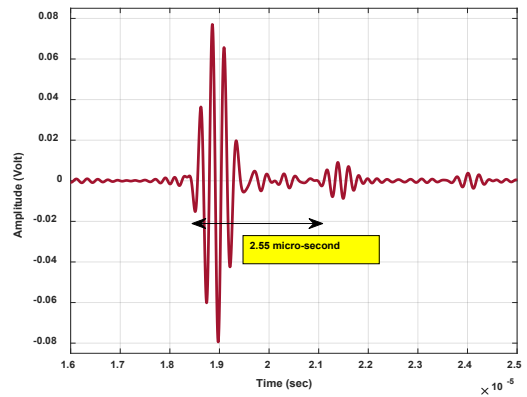Figure 10. Notch on the wedge, 7.5 mm distance from the other side of the wedge.

Figure 11. Signal reflected from the notch.

3. FEATURE EXTRACTION METHODOLOGY

This section presents a three-step approach for feature extraction, that will be used as input vector to train the NN model in the subsequent section. Firstly, the signals obtained from the wedge test are subjected to a cleaning procedure. Subsequently, these signals are smoothened, enveloped, and the peaks of the resulting curves are identified as illustrated in Figure 12. The algorithms of smoothing, enveloping and peak finding are discussed in Subsections 3.1 - 3.3.

3.1 Data Smoothing by Using Moving Average Algorithm

In a moving average algorithm, given an input time-series signal X_n with length N, where $n = 0, 1, 2, \ldots, N-1$, we can define the moving average window size as M, which represents the number of adjacent samples that are considered for smoothing. The moving average algorithm is described taking the following steps:

a. Initialize the smoothed signal y_n as an array of zeros with the same length as X_n.
b. For each sample index n from $M/2$ to $N - (M/2)$ (both inclusive), compute the moving average for the current sample index as:

$$y_n = \frac{1}{M} \sum X_{n-\frac{M}{2}+K^2} \tag{5}$$

where $K = 0, 1, 2, \ldots, M-1$.

c. For sample indices outside the range $M/2$ to $N - (M/2)$, we can either pad the signal with zeros or adjust the range accordingly to fit the available samples.
d. The resulting smoothed signal y_n represents the moving average of the original signal X_n.

It is important to note that this mathematical representation assumes a symmetric moving average window, where an equal number of samples is considered on both sides of the current sample.

3.2 Envelop Finding Algorithm

The algorithm for finding the envelope of a time-series signal is described in mathematical notation as follows. Given an input time-series signal X_n with length N, where $n = 0, 1, 2, \ldots, N-1$, the following steps are taken:

a. It is recommended to implement this algorithm after pre-processing steps such as smoothing or filtering on the input signal X_n to reduce noise, fluctuations and also obtain more reliable results.
b. Compute the upper envelope of the signal, which represents the maximum values at each point in time. Denote the upper envelope as U_n.
   i. Initialize U_n as an array of zeros with the same length as X_n.
   ii. For each sample index n from 1 to $N-2$, perform the following steps:
      • If X_n is greater than both X_{n-1} and X_{n+1}, set U_n equal to X_n.
      • Otherwise, set U_n equal to the maximum value between U_{n-1} and U_{n+1}.
   iii. For the sample indices $n = 0$ and $n = N-1$, set U_n equal to the maximum value between U_{n+1} and U_{n-1}, respectively.

3.2 Peak Finding Algorithm

The algorithm for finding peaks in the envelope of a time-series signal is described in mathematical formalism as follows. Given an input envelope signal E_n of length N, where $n = 0, 1, 2, \ldots, N-1$, the following steps are taken:

a. Define a threshold value T that represents the minimum amplitude difference required for peak detection.
b. Initialize an empty array to store the indices of the detected peaks, denoted as P.
c. For each sample index n from 1 to $N-2$, if E_n is greater than both E_{n-1} and E_{n+1} by at least the threshold T, add n to the array P as a detected peak.
d. The array P contains the indices of the detected peaks in the envelope signal E_n.
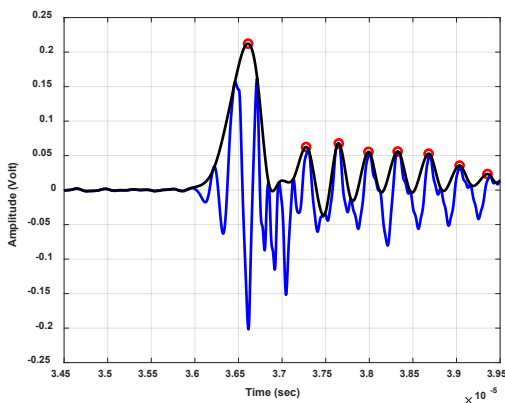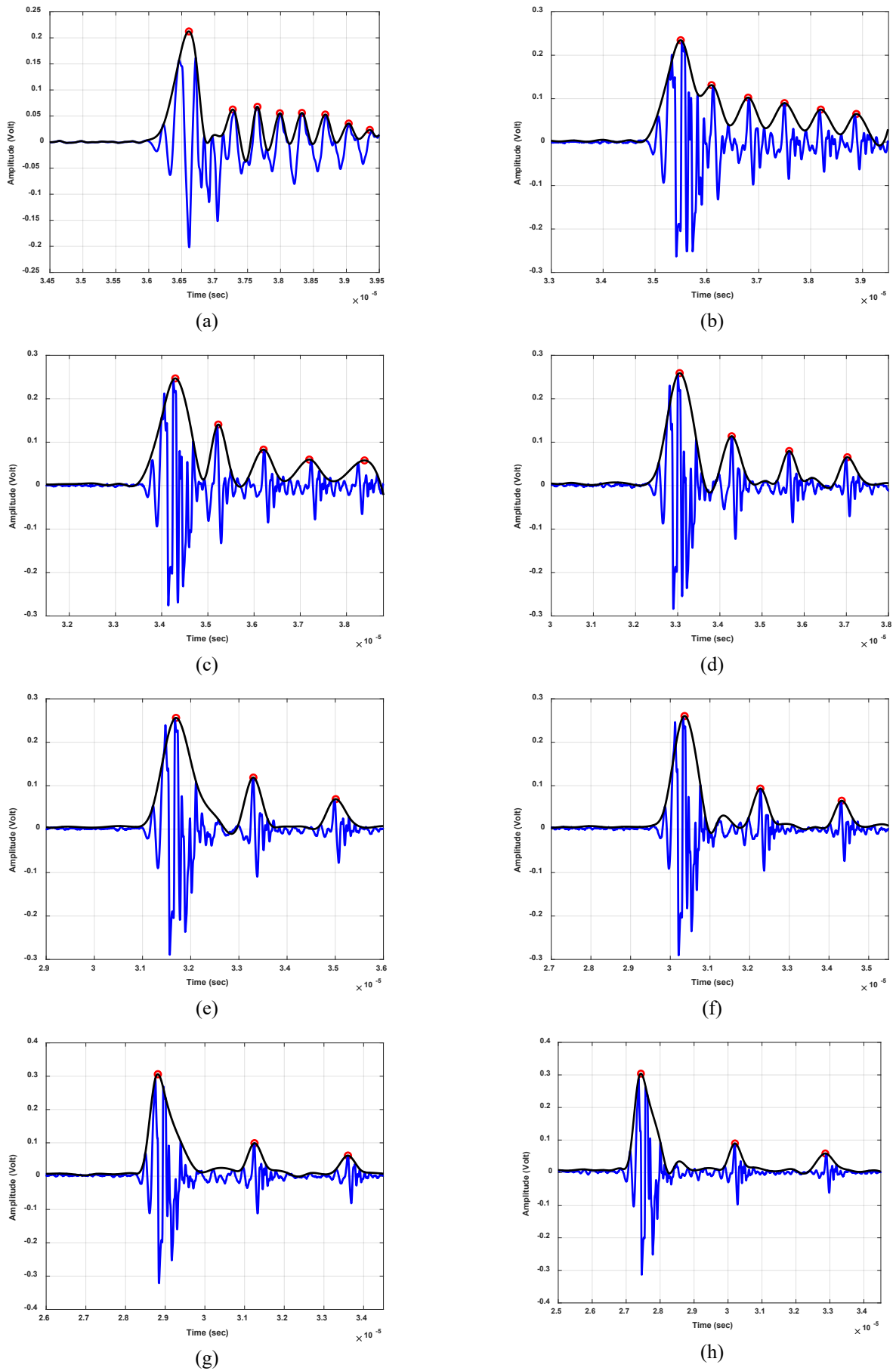

(a)
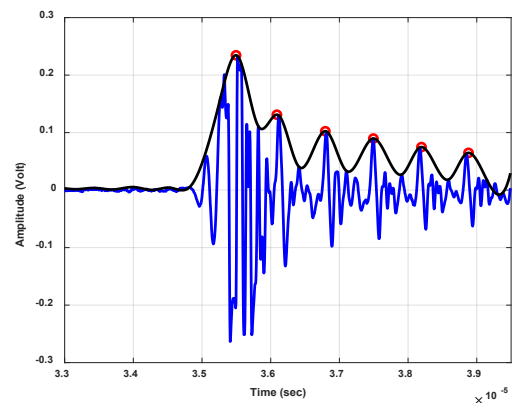
(b)

Figure 12. Time difference between the consecutive peaks shown by red dot, (a) 1 mm; (b) 2 mm; (c) 3 mm; (d) 4 mm; (e) 5 mm; (f) 6 mm; (g) 7 mm; (h) 8 mm.
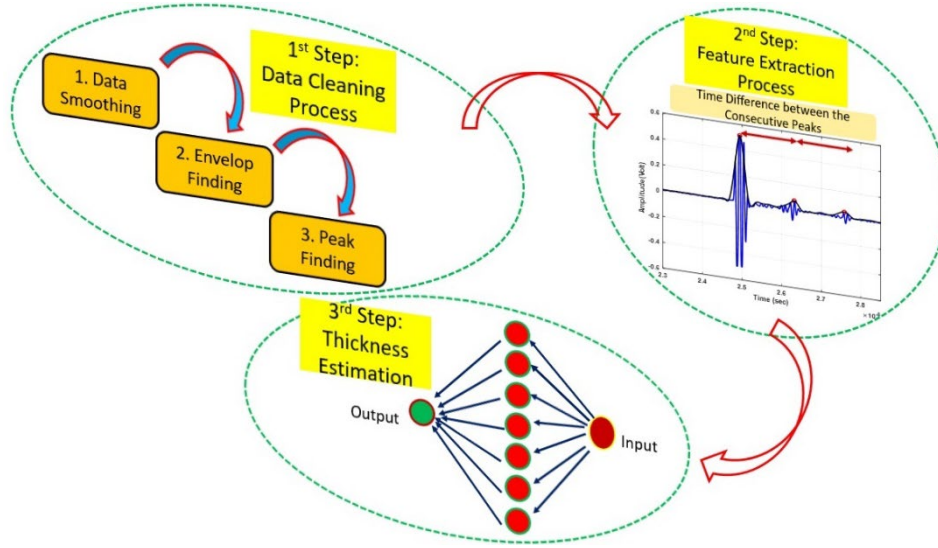
Figure 13. Workflow diagram of the thickness prediction process.

4. MATERIAL THICKNESS PREDICTION BY NEURAL NETWORK

After finding the peaks, the time difference between the consecutive peaks is set as input of the neural network as the outcome of feature extraction process, and it predicts the corresponding sample thicknesses for each set of signals as its output. The entire thickness prediction process that includes data cleaning, feature extraction and neural network training are shown in Figure 13 as a workflow diagram. The neural network contains one neuron at the input layer (the vector of time differences between the consecutive peaks) and 7 neurons at the hidden layer and one neuron at the output layer which represents the predicted sample thickness. The mathematical relationships between input and output of the neural network are written as:

Input-to-Hidden Layer
$$H = tanh\ (w_1 \times Y + b_1) \tag{6}$$

Hidden Layer-to-Output
$$Predicted\ Thickness = (w_2 \times H + b_2) \tag{7}$$

where Y is the input vector of time differences between the consecutive peaks.

By using the steepest descent gradient method to update the weights and biases, and after completion of neural network training with 450 training epochs and learning rate of 0.01, the given time difference between the peaks at the input of the neural network will return predicted sample thickness at the output of the neural network. Any given pre-processed set of signals to the input of the neural network will be interpolated regarding the value laid within the range between minimum and maximum values i.e., 1 mm - 8 mm. The results of the neural network training are shown in Figure 14. In Equations (6) and (7), w_1 is the weight vector between input and hidden layer, b_1 is the bias vector in hidden layer, w_2 is the weight vector between hidden layer and output, and b_2 is the bias term at the output.

In order to evaluate the performance of the trained neural network, two different samples with 3.15 mm and 4.2 mm thicknesses were chosen to test the neural network. The following results were obtained as outputs of the trained network. As seen in Table 2, the predicted thicknesses are very close to the measured values.
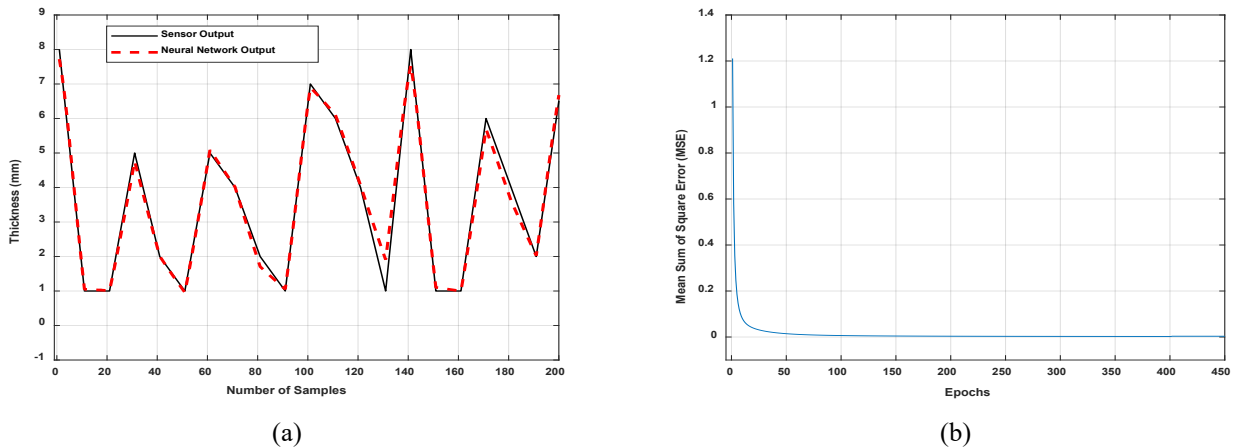

(a)

(b)

Figure 14. (a) Thickness prediction by neural network after training process; (b) Mean sum of square error (MSE) after 450 training epochs.

Table 2. Comparison between measured values by sensor for test samples and the predicted values by neural network.

Nominal Values (mm)	Predicted Values by Neural Network (mm)	Error (%)
3.15	3.07	2.53
4.2	4.1	2.38

4.1 Void Detection by Neural Network

For this purpose, a sample with a defined thickness of 4 mm was chosen as seen in Figure 15(a), and a mobile set-up was designed and developed to position the sensor holder over the pre-drilled holes made in the sample as illustrated in Figures 15(b) and 15(c). The drilled holes were made to represent the voids in the sample. Out of these holes, three were chosen at varying distances from the other side of the sample i.e., 1.6 mm, 2.2 mm and 3.9 mm for the purpose of training the neural network as shown in Figure 16(a), while the remaining three were chosen at varying distances from the top of the sample i.e., 2.5 mm, 2.9 mm and 3.7 mm for testing the trained neural network. A laser pointer was installed on the moving platform rod to align the sensor position on the holes.

Similarly, the time difference between the consecutive peaks is set as input of the neural network, and it predicts the corresponding distances from the top surface of the sample to the initial position of the holes as its output. Figure 17 shows the corresponding curves for the three holes which are used for training the neural network. For this problem, a neural network was assigned with one neuron at the input layer (time difference between the consecutive peaks) and 7 neurons at the hidden layer and one neuron at the output layer which represents the predicted initial position of the holes. The neural network was trained after 500 training epochs with the learning rate of 0.01, the given time difference between the peaks at the input of the neural network will return predicted position of the voids at the output of the neural network. Any given pre-processed set of signals to the input of the neural network will be interpolated according to the value laid within the range between minimum and maximum values i.e., 1 mm – 4 mm. The results of the neural network training are shown in Figure 18.

To evaluate the performance of the trained neural network, three different samples with 2.5 mm, 2.9 mm and 3.7 mm were chosen to test the neural network. The following results were obtained as outputs of the trained network. As seen in Table 3, the predicted positions demonstrate good agreement with the nominal values.
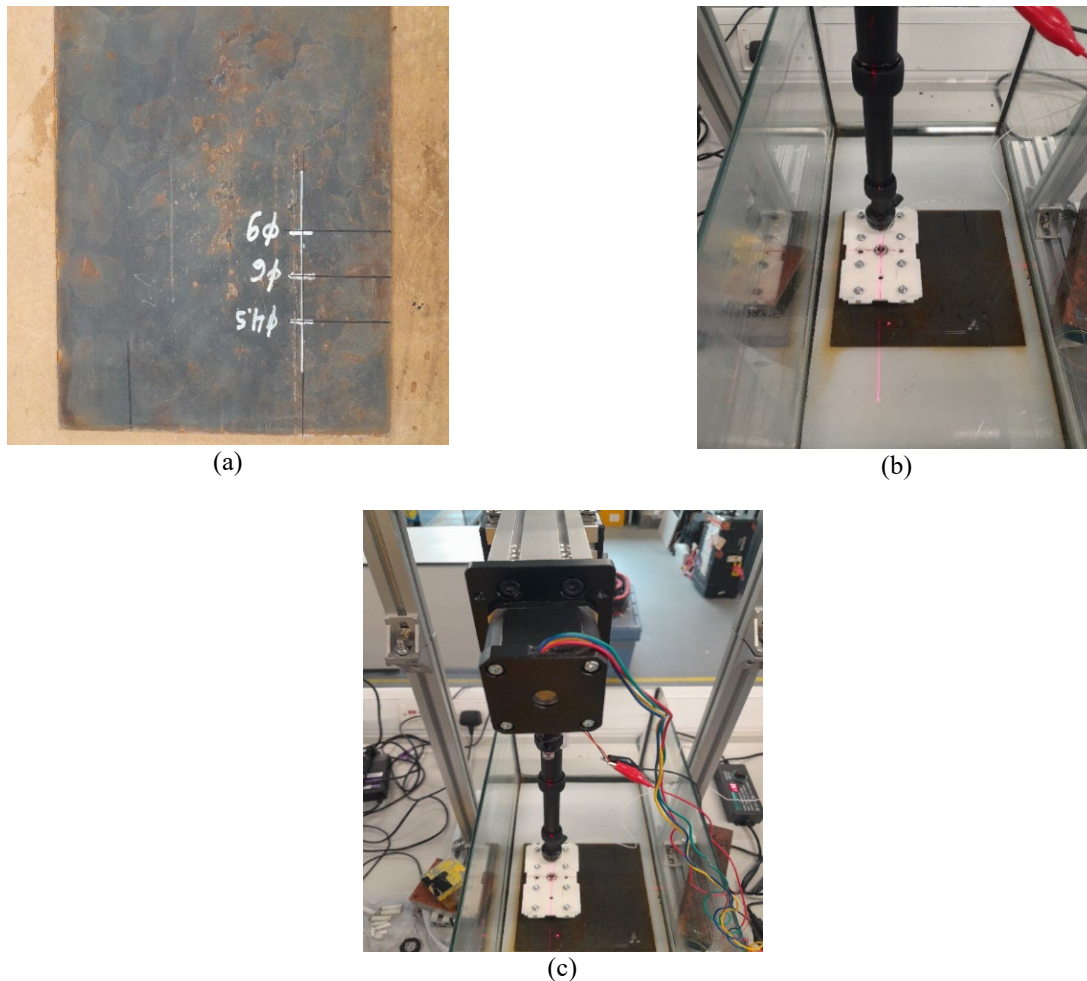

(a)

(b)

(c)

Figure 15. (a) Sample with 4.2 mm thickness; (b) Moving set-up with laser pointer; (c) Step motor to move the platform.
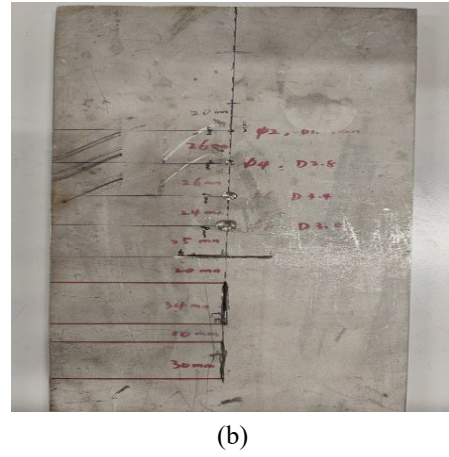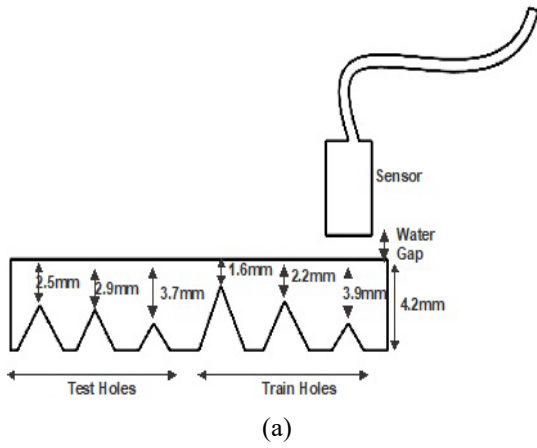
(a)

(b)

Figure 16. (a) Three train holes besides three test holes on steel sample; (b) Sample with holes.
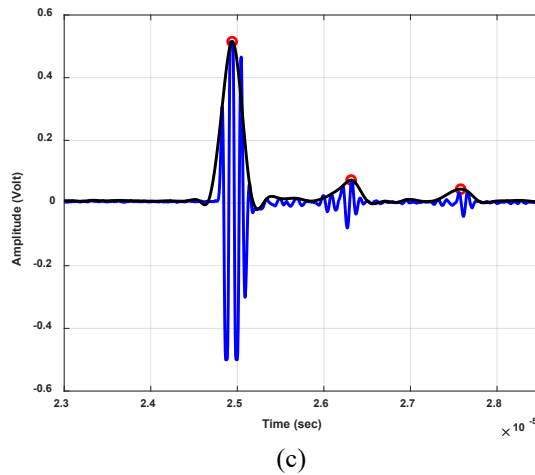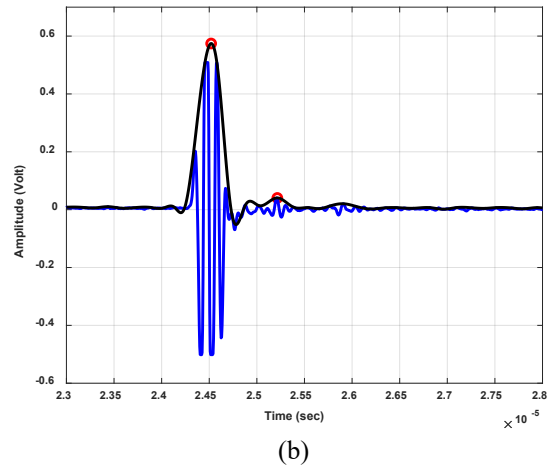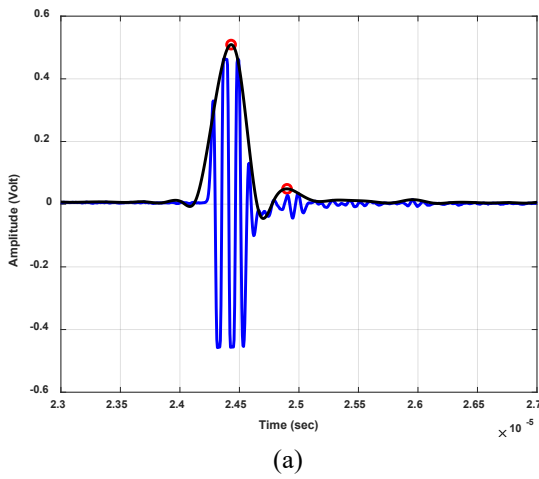

(a)

(b)

(c)

Figure 17. Time difference between the consecutive peaks shown by red dot and hole with a certain distance from top of the sample, (a) 1.6 mm; (b) 2.2 mm; (c) 3.9 mm.
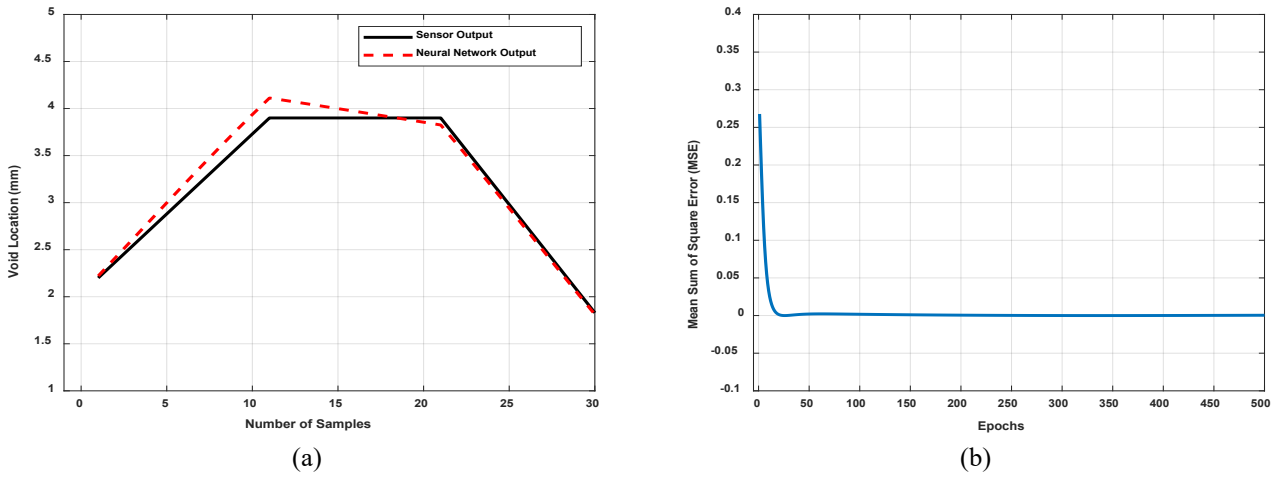
Figure 18. (a) Position prediction by neural network after training process; (b) Mean sum of square error (MSE) after 500 training epoch.

Table 3. Comparison between measured values by sensor for test samples and the predicted values by neural network.

Nominal Values (mm)	Predicted Values by Neural Network (mm)	Error (%)
2.5	2.64	5.6
2.9	3.05	5.2
3.7	3.96	7.0

5. RESULTS AND DISCUSSION

In this study, we developed a feature extraction method and a predictor neural network applied for some samples made of steel material with specific geometries, which can be highlighted as a notable limitation of this method. The feature extraction process included the selection of characteristics from ultrasonic sensor data exclusively for the unique properties of the mentioned material. Similarly, the neural network architecture and parameters were optimized to work efficiently with the material and geometric properties of the samples. As a result, the functionality of this approach might be constrained to the particular material type and geometry, limiting its generalization to other samples with different materials and geometry. Despite the fact that the proposed method has some limitations, it is worth mentioning that the measurement and prediction methods for a specific application is a common engineering practice in different industry sectors. Therefore, our goal in this study was to showcase the feasibility and accuracy of the approach for a particular material, laying the foundation for future work to generalize the method to different materials through proposing novel data processing techniques and neural network architectures.
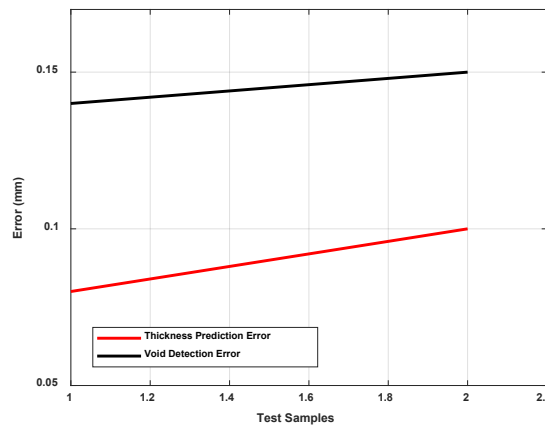

Figure 19. Thickness prediction error and void detection error by neural networks.

In spite of the limitations mentioned above, the results demonstrate an acceptable level of agreement between the nominal thickness values and the predicted values by the neural network. Figure 19 shows the error values for both thickness prediction and void detection. As shown, the average error values of 80 microns and 140 microns have been obtained for thickness prediction and void detection, respectively. The remarkable level of agreement between nominal and predicted values proves the effectiveness of the approach for the targeted material sample. The outcome of this study can contribute to the applications where precise thickness measurement is required.

6. CONCLUSIONS

This study demonstrates the integration of ultrasonic sensors and neural networks particularly for the application of material thickness measurement and void detection. The methodology discussed in this study offers non-invasive, real-time, and highly accurate results, reducing shortcomings of traditional methods. Through time-series analysis and predictive modelling, we demonstrated that neural networks can effectively capture nonlinear relationships between ultrasonic data and material thickness. This innovative approach enables real-time monitoring for a variety of industrial applications. This study aimed to illuminate the potential of integrating ultrasonic sensing and neural networks for further advancements in non-destructive testing and quality control.

ACKNOWLEDGEMENT AND FUNDING

DECLARATION OF CONFLICTING INTERESTS

The authors wish to confirm that there are no known conflicts of interest associated with this publication and there has been no significant financial support for this work that could have influenced its outcome. The authors also confirm that they have given due consideration to the protection of intellectual property associated with this work and there are no impediments to publication, including the timing of publication, with respect to intellectual property. In so doing, the authors confirm that they have followed the regulations of their institutions concerning intellectual property.

REFERENCES

[1]   D. K. Hsu and M. S. Hughes, Simultaneous ultrasonic velocity and sample thickness measurement and application in composites, *The Journal of Acoustical Society of America*, 92(2), 1992, 669-675.

[2]   V. Hassani and T. Tjahjowidodo, A hysteresis model for a stacked-type piezoelectric actuator, *Journal of Mechanics of Advanced Materials and Structures*, 24(1), 2017, 73-87.

[3]   V. Hassani and T. Tjahjowidodo, Integrated rate and inertial dependent Prandtl-Ishlinksii model for piezoelectric actuator, *2nd International Conference on Instrumentation Control and Automation*, Bandung, Indonesia, 2011, 152-157.

[4]   Ultrasound and Ultrasonic Testing, Iowa State University, Centre for Non-Destructive Evaluation. https://www.nde-ed.org/NDETechniques/Ultrasonics/Ultrasound.xhtml (accessed 14.03.2024).

[5]   N. Xia, P. Zhao, T. Kuang, Y. Zhao, J. Zhang and J. Fu, Nondestructive measurement of layer thickness in water-assisted coinjection-molded product by ultrasonic technology, *Journal of Applied Polymer Science*, 135, 2018, 46540.

[6]   J. Zhang, Y. Cho, J. Kim, A. Malikov, Y. H. Kim, J. -H.Yi and W. Li, Non-destructive evaluation of coating thickness using water immersion ultrasonic testing, *Journal of Coatings*, 11(11), 2021, 1421.

[7]   H. Du, H. Fan, Q. Zhang and S. Li, Measurements of the thickness and area of thick oil slicks using ultrasonic and image processing methods, *Journal of Remote Sensing*, 15(12), 2023, 2977.

[8]   K. Ikeda, N. Yusa, T. Tomizawa and H. Song, Reliability analysis of pipe wall thinning basd on quantification of ultrasonic testing, *Proceedings of the 13th European Conference on Non-Destructive Testing (ECNDT),* Lisbon, Portugal, 2023.

[9]   H. Zhu, J. Tu, C. Cai, Z. Deng, Q. Wu and X. Song, A fast signal-processing method for electromagnetic ultrasonic thickness measurement of pipelines based on UKF and SMO, *Journal of Energies*, 15(18), 2022, 6554.

[10] Y. Chen, J. Zhang, A. J. Croxford and P. D. Wilcox, Thickness measurement optimisation for permanently installed inductively coupled ultrasonic transducer systems, *Journal of NDT & E International*, 129, 2022, 102655.

[11] A-scan, B-scan, and C-scan Ultrasonic Data from Robotic Inspections, 2021. https://blog.geckoroboticks.com/unpacking-a-scans-b-scans-and-c-scans-in-robotic-ultrasonic-inspection.

[12] K. Yadav, R. Kumar, N. Dhiman, S. Yadav and P. K. Dubey, Development and study of ultrasonic immersion testing system for industrial and metrological application, *Journal of Instrumentation*, 18(3), 2023, 03001.

[13] J. D. Eckels, E. M. Jacobson, I. T. Cummings, I. F. Fernandez, K. Ho, N. Dervilis, E. B. Flynn and A. J. Wachtor, Predicting local material thickness from steady-state ultrasonic wavefield measurements using a convolutional neural network, *Journal of Ultrasonics*, 123, 2022, 106661.

[14] C. C. Aggarwal, *Neural Networks and Deep Learning: A Textbook*, Springer International Publishing, 2018.

[15] F. Chollet, Xception: Deep learning with depthwise separable convolutions, *Proceedings of the IEEE Conference on Computer Vision and Pattern Recognition*, Honolulu, USA, 2017, 1800-1807.

[16] S. Hochreiter and J. Schmidhuber, Long short-term memory, *Journal of Neural Computation*, 9(8), 1997, 1735-1780.

[17] J. Mi, J. Yu and G. Huang, Direct-drive electro-hydraulic servo valve performance characteristics prediction based on big data and neural networks, *Sensors*, 23(16), 2023, 7211.

[18] P. Yu, H. Wang and J. Cao, Aero-engine residual life prediction based on time-series residual neural networks, *Journal of Intelligent and Fuzzy Systems*, 45(2), 2023, 2437-2448.

[19] Y. Liu, Dynamics evolution prediction from time series data with recurrent neural networks in a complex system, *International Journal of Modern Physics C*, 34(08), 2022, 2350099.

[20] X. Xu, X. Zhai, A. Ke, Y. Lin, X. Zhang, Z. Xie and Y. Lou, Prediction of leakage pressure in fractured carbonate reservoirs based on PSO-LSTM neural network, *Journal of Processes*, 11(7), 2023, 2222.

[21] W. Li, L. Wang, Z. Dong, R. Wang and B. Qu, Reservoir production prediction with optimized artificial neural network and time series approaches, *Journal of Petroleum Science and Engineering*, 215(4), 2022, 110586.

[22] Z. Li, D. Yang and G. Yin, Ship flooding time prediction based on composite neural network, *Journal of Marine Science and Engineering*, 11(6), 2023, 1123.

[23] L. Zhao and M. A. L. Bell, A review of deep learning applications in large ultrasound imaging of COVID-19 patients, *BMEF: A Science Partner Journal*, 2022, 9780173.